4

Blind Space-Time Signal Processing

Arogyaswami J. Paulraj
Constantinos B. Papadias
Vellenki U. Reddy
Alle-Jan van der Veen

As discussed in Chapters 1–3, signal processing functions in wireless communications include modulation/demodulation, channel coding/decoding, channel equalization and estimation of transmitted signals, and reduction of cochannel interference (CCI). One promising approach to improve signal processing performance is space-time (S-T) processing, which operates simultaneously on multiple antennas. A key leverage of this spatial dimension is CCI reduction. This reduction is possible since the CCI and the desired signal almost always arrive at the antenna array (even in complex multipath environments) with distinct and often well-separated spatial signatures, thus allowing the modem to exploit this difference to reduce the CCI. Likewise, the space-time transmit processing can use spatial selectivity to deliver signals to the desired mobile while minimizing the interference for other mobiles. Another leverage is the exploitation of blind methods. Use of training for equalization consumes bandwidth and is not efficient in rapidly time-varying channels. Therefore, blind channel equalization and estimation of multiple users' signals can improve network capacity and performance.

The spatial dimension can also be used to enhance other aspects of space-time modem performance. In reception, the antennas can be used to provide enhanced array gain, improve signal to thermal noise ratio, and enhance diversity gain, as discussed in Chapter 1. In transmission, the spatial dimension can enhance array gain, improve transmit diversity, as is also discussed in Chapter 1, and reduce delay spread.

The chapter focuses on the receiver S-T processing for nonspread modulation and is organized as follows. In Section 4.1, we summarize the propagation model. In Section 4.2, we develop a model for signals received at an antenna array and discuss the spatial and temporal structures in this model. In Section 4.3, we discuss a zero-forcing view of channel identifiability and equalizability and discuss the similarities and differences between intersymbol interference (ISI) and CCI cancellation. In Section 4.4, we present some recently proposed techniques for blind multiuser detection using block and recursive techniques. Section 4.5 concludes with a summary of the chapter.

4.1 The Wireless Propagation Environment

As discussed in earlier chapters, the propagation of radio signals on both the forward (base-station-to-subscriber unit) and reverse (subscriber unit-to-base-station) links is affected by a channel in several ways. Multipath propagation results in the spreading of the signal in three dimensions. These are the delay (or time) spread, Doppler (or frequency) spread and angle spread. These spreads (see Figure 4.1) have significant effects on the signal and are summarized below together with the terminology we will use in this chapter.

Doppler Spread: Time-Selective Fading. Doppler spread results from mobile motion and local scattering near the mobile. If one assumes uniformly dis-

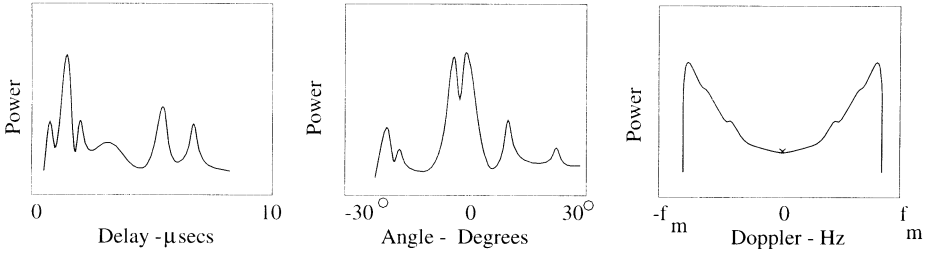

Figure 4.1 The three spreads of the wireless channel.

tributed local scatterers, then, as discussed in Chapter 2, the baseband power spectrum of the received vertical electrical field due to a continuous-wave tone has a U-shaped form, called the classical (or Jakes' model) spectrum [9].

If there is a direct line-of-sight path, the channel spectrum is modified by an additional line at a frequency corresponding to the relative velocity between the base and the mobile. Doppler spread causes time-selective fading and can be characterized by the *coherence time* of the channel. The larger the Doppler spread, the smaller the coherence time.

Delay Spread: Frequency-Selective Fading. Due to the multipath propagation, several time-shifted and scaled versions of the transmitted signal will arrive at the receiver. Typically, a double negative exponential model is observed: the delay separation between paths increases negative exponentially with path delay, and the path amplitudes also fall off negative exponentially with delay. This spread of path delay is called *delay spread*. Delay spread causes frequency-selective fading and is also measured in terms of *coherence bandwidth*. The larger the delay spread, the smaller the coherence bandwidth.

Angle Spread: Space-Selective Fading. Angle spread on receive refers to the spread of arrival angles of the multipaths at the antenna array. Likewise, angle spread in transmit refers to the spread of departure angles of the multipaths. The angle of arrival (or departure) of a path can be statistically related to the path delay. With a constant-delay, ellipse-scattering model, it can be shown that angle spread is proportional to delay spread and inversely proportional to the transmitter-receiver separation. Angle spread causes space-selective fading and is characterized by the *coherence distance*. The larger the angle spread, the shorter the coherence distance.

Multipath Propagation in Large Cells. Multipath scattering underlies the three spreading effects described above and Doppler spread, which in addition requires subscriber unit motion. It is important to understand the types of scatterers and their contribution to channel behavior. These scatterers are illustrated in Figure 4.2.

Scatterers Local to Mobile. Scattering local to the mobile is caused by buildings in the vicinity of the mobile (a few tens of meters). Mobile motion and local scattering give rise to Doppler spread, which causes time-selective fading. For a mobile traveling at 65 mph, the Doppler spread is about ± 200 Hz in the 1900 MHz band. Although local scattering contributes to Doppler spread, the delay

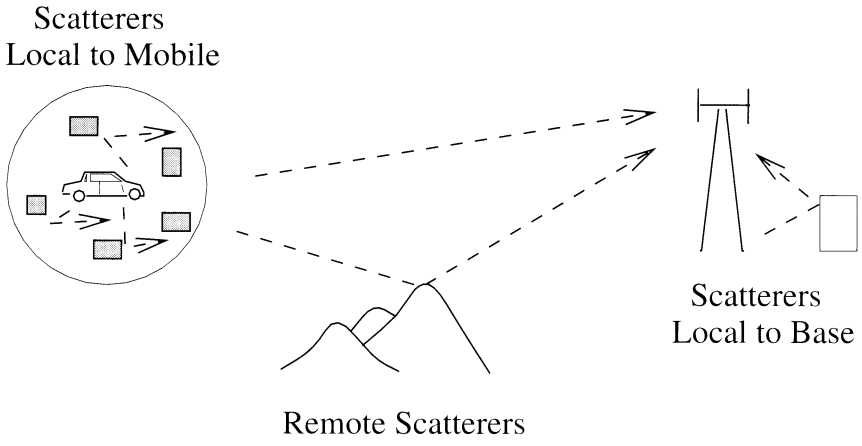

Figure 4.2 Multipath propagation has three distinct scattering sources, each of which gives rise to different channel effects.

spread will usually be insignificant because of the small scattering radius. Likewise, the angle spread will also be small.

Remote Scatterers. The emerging wavefront from the local scatterers may then travel directly to the base or may be scattered toward the base by remote *dominant scatterers*, giving rise to specular multipath. These remote scatterers can be either terrain features or high-rise building complexes. Remote scattering can cause significant delay and angle spreads.

Scatterers Local to Base. Once these multiple wavefronts reach the base station, they may be scattered further by local structures such as buildings or other structures that are in the vicinity of the base. Such scattering will be more pronounced for low elevation and below-rooftop antennas. The scattering local to the base can cause severe angle spread, which in turn can cause space-selective fading. This fading is coherent, unlike the time-varying, space-selective fading caused by remote scattering.

Space-Time Channel Model. A multipath channel [9] is illustrated in Figure 4.3. Typical path amplitude, delay, and fading statistics can be obtained from published propagation models. The signal from the mobile travels through a number of paths, each with its own power fading and delay. The fading can be either Rayleigh or Rician and can have a Doppler spectrum that is flat or classical. These paths arrive at the receive antenna array with varying angles of arrival. The composite multipaths induce a different multipath channel at each antenna because of differences in relative phasing of the paths.

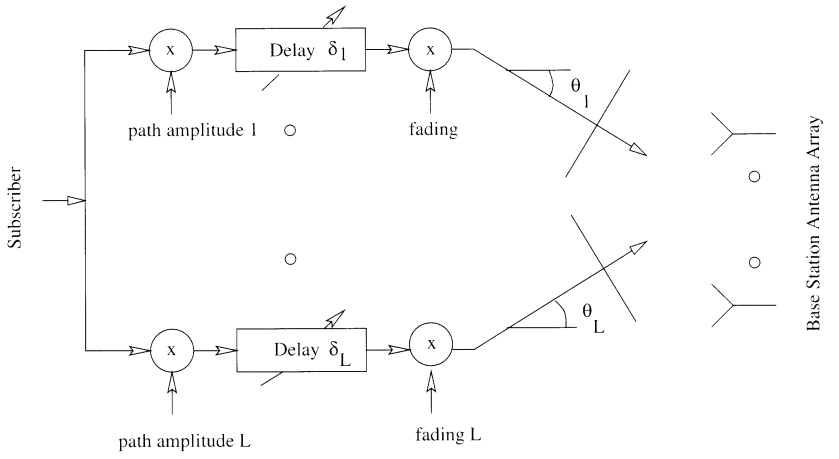

Figure 4.3 Multipath model.

A typical example of a macrocellular channel in a hilly terrain in the case of the European cellular system GSM (Groupe Speciale Mobile) is shown in Figure 4.4. We plot the frequency response at each antenna. Since the channel bandwidth is high (200 KHz), the channel is highly frequency-selective in a hilly terrain environment where delay spreads can reach 10 to 15 μs. Also, the large angle spread causes variations of the channel from antenna to antenna. The channel variation in time depends upon the Doppler spread. Note that since GSM uses a short time slot, the channel variation during the time slot is negligible.

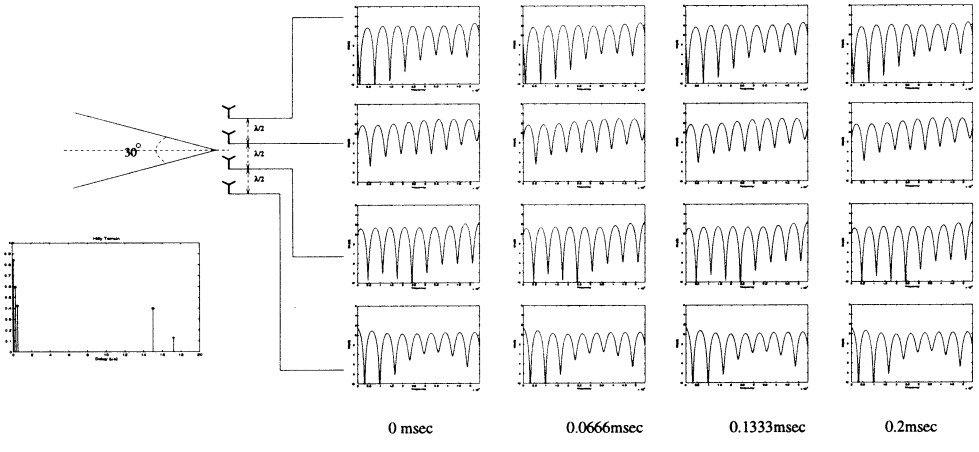

Figure 4.4 Channel frequency response at four different antennas for GSM.

4.2 Signal Model and Structure

In this section, we describe analytical models for the received signals at the antenna elements in a wireless system.

4.2.1 Signal Model

In this section, we develop suitable receive signal models for the single and multiple user cases shown in Figure 4.5. First, we develop the single-user (SU) model and later extend it to the multiple-user (MU) case. In both cases, on the reverse link, the subscriber uses a single antenna input (SI) and base station uses multiple antenna outputs (MO).

Let $c(t)$ denote the continuous-time impulse response of the multipath channel to an omnidirectional antenna (excluding that of transmitter and receiver filters), which we refer to as the physical channel impulse response. Assuming a specular multipath model of the type considered in earlier chapters, we can express $c(t)$ as

$$c(t) = \sum_{l=1}^{L} \alpha_l(t)\delta(t - \tau_l), \tag{4.1}$$

where $\alpha_l(t)$ and τ_l denote the complex path fading and the propagation delay of lth path, respectively, L is the number of multipaths, and $\delta(\cdot)$ is the Dirac delta function.

Let $u(t)$ denote the baseband equivalent of the transmitted signal that depends on the modulation waveform and the information data stream. In the IS-54 TDMA standard, $u(\cdot)$ is a $\pi/4$-shifted DQPSK (differential quadrature phase-shift keying), gray-coded signal that is modulated by a pulse with square-root raised

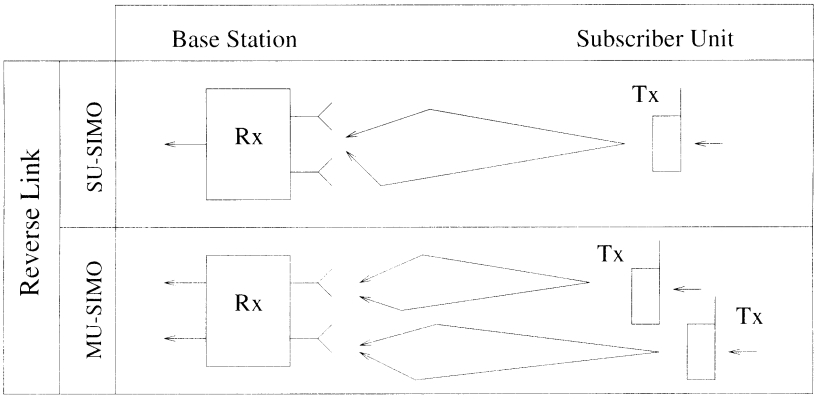

Figure 4.5 Single and multiple user receive configurations.

cosine spectrum with excess bandwidth of 0.35. In GSM, a Gaussian minimum shift keying (GMSK) modulation is used. See [4, 13, 33] for more details.

For a linear modulation (e.g., DQPSK), we can write

$$u(t) = \sum_k g(t - kT)s(k), \tag{4.2}$$

where $s(k)$ denote the transmitted symbols, T denotes the baud (or symbol) period, and $g(t)$ denotes the effective continuous-time pulse shape that includes the effects of the transmitting and receiving filters.

We now consider an m-element antenna array. We can express the noiseless baseband signal at the ith element of the array, $x_i(t)$, as

$$x_i(t) = \sum_{l=1}^{L} a_i(\theta_l)\alpha_l(t)u(t - \tau_l), \tag{4.3}$$

where $a_i(\theta_l)$ is the response of the ith sensor for an lth path from direction θ_l, and $\alpha_l(t)$ represents the complex path fading for the lth path. We can rewrite (4.3) as

$$x_i(t) = \sum_k \sum_{l=1}^{L} a_i(\theta_l)\alpha_l(t)g(t - \tau_l - kT)s(k) \tag{4.4}$$

In the above model, we have assumed that the inverse of the signal bandwidth is large compared to the travel time across the array (and that the channel fading bandwidth is assumed to be negligible compared to the signal bandwidth). This is the so-called narrowband assumption of the transmitted signal. Therefore, the signal complex envelope received by each antenna is identical except for phase (and perhaps amplitude) differences that depend on the path angle-of-arrival. This angle-of-arrival dependent phase shift along with any amplitude-phase response differences is included in $a_i(\theta_l)$ [19]. The complex reverse link signal fading amplitude $|\alpha_l(t)|$ is Rayleigh- or Rician-distributed.

The channel model described above uses physical path parameters such as path gain, delay, and angles-of-arrival, none of which are known nor are easily estimated. The noiseless baseband signal received at the ith antenna output can also be written as

$$x_i(t) = \sum_k h_i(t - kT)s(k), \tag{4.5}$$

where $h_i(t)$ represents the composite baseband impulse response of the channel from the user's transmitter to the output of the ith sensor and is the convolution of the physical channel impulse response and the pulse shaping function. Since $h_i(t) = c_i(t) * g(t)$, it follows that

$$h_i(t) = \sum_{l=1}^{L} a_i(\theta_l)\alpha_l(t)g(t - \tau_l) \qquad i = 1,\ldots, m. \tag{4.6}$$

This impulse response $h_i(t)$ has a finite duration called the channel length. In the following, we assume that the fading coefficients $\{\alpha_l\}$ remain constant over the time interval during which we collect the data and therefore treat $h_i(t)$ as time-invariant. Defining the vector impulse response[1] $\mathbf{h}(t) = [h_1(t) \ \cdots \ h_m(t)]^T$, (4.6) can be written as

$$\mathbf{h}(t) = \sum_{l=1}^{L} \mathbf{a}(\theta_l)\alpha_l(t)g(t - \tau_l), \tag{4.7}$$

where $\mathbf{a}(\theta) = [a_1(\theta) \ \cdots \ a_m(\theta)]^T$ is the array response vector.

Sampling $h_i(t)$ at the symbol rate, we get $h_i(n) = h_i(t)\big|_{t=t_0+nT}$, which is called the symbol-spaced channel, where t_0 is the initial sampling instant. The symbol-rate sampled received signal at the output of the ith antenna element can be expressed as

$$x_i(k) = \sum_{n=0}^{N-1} h_i(n)s(k - n), \qquad i = 1,\ldots, m, \tag{4.8}$$

where we have assumed, without loss of generality, the impulse response corresponding to each antenna to span N symbol periods (corresponding to a channel length of NT). Again, defining the array output $\mathbf{x}(k) = [x_1(k) \ \cdots \ x_m(k)]^T$, we can rewrite (4.8) as

$$\mathbf{x}(k) = \sum_{n=0}^{N-1} \mathbf{h}(n)s(k - n), \tag{4.9}$$

where $\mathbf{h}(n) = \mathbf{h}(t)\big|_{t=t_0+nT}$. If we define H as

$$H = [\mathbf{h}(0) \ \cdots \ \mathbf{h}(N - 1)], \tag{4.10}$$

(an $m \times N$ channel matrix), then (4.9) can be rewritten as

$$\mathbf{x}(k) = H\mathbf{s}(k), \tag{4.11}$$

where

$$\mathbf{s}(k) = \begin{bmatrix} s(k) \\ \vdots \\ s(k - N + 1) \end{bmatrix}. \tag{4.12}$$

In terms of the physical channel parameters and the pulse shaping function, H can be expressed as

$$H = \mathbf{A}(\theta)\Lambda\mathbf{G}(\tau), \tag{4.13}$$

where $A(\theta) = [\mathbf{a}(\theta_1) \ \ \mathbf{a}(\theta_2) \ \cdots \ \mathbf{a}(\theta_L)]$, $\Lambda = \text{diag}\{\alpha_1, \cdots, \alpha_{L-1}, \alpha_L\}$ and

[1]The superscript ^{T} denotes the transpose operator.

$$\mathbf{G} = \begin{bmatrix} g(t_0 - \tau_1) & g(t_0 + T - \tau_1) & \cdots & g(t_0 + NT - T - \tau_1) \\ \vdots & \vdots & \cdots & \vdots \\ g(t_0 - \tau_{L-1}) & g(t_0 + T - \tau_{L-1}) & \cdots & g(t_0 + NT - T - \tau_{L-1}) \\ g(t_0 - \tau_L) & g(t_0 + T - \tau_L) & \cdots & g(t_0 + NT - T - \tau_L) \end{bmatrix}. \tag{4.14}$$

In the following, we refer to the rows of H as the subchannel responses. From (4.13) we get the following expression for each coefficient of H in terms of the channel parameters [32]:

$$H_{ij} = \sum_{l=1}^{L} \alpha_l a_i(\theta_l) g(t_0 - \tau_l + (j-1)T). \tag{4.15}$$

As we will see later, there are advantages if $h_i(t)$ is sampled at a rate greater than the symbol rate. This oversampling can be easily incorporated in our signal model. Let the fractional sampling interval be $T_s = T/P$, where P is an integer. We define the pth phase, $p = 1, 2, \ldots, P$, of the fractionally spaced response channel corresponding to ith antenna as

$$\mathbf{h}_p(n) = \mathbf{h}(t)\,\big|_{t=t_0+nT+\frac{(p-1)}{P}T}. \tag{4.16}$$

Now, the new $mP \times 1$ vector channel impulse response can be redefined as

$$\mathbf{h}(n) = \begin{bmatrix} \mathbf{h}_1(n) \\ \vdots \\ \mathbf{h}_P(n) \end{bmatrix}. \tag{4.17}$$

Similarly to (4.16), we define the pth phase of the vector received signal $\mathbf{x}_p(k)$ as

$$\mathbf{x}_p(n) = \sum_{n=0}^{N-1} \mathbf{h}_p(n) s(k-n), \tag{4.18}$$

where we have assumed again, for convenience, that the impulse response of each phase spans N symbol periods. H (now of dimension $mP \times N$) will correspond to a fractionally spaced vector channel with number of subchannels as mP and each channel length as N, and will still obey the definition (4.10) with $\mathbf{h}$ given in (4.17). The channel model is again

$$\mathbf{x}(k) = H\mathbf{s}(k), \tag{4.19}$$

with $\mathbf{x}(k) = [\mathbf{x}_1^T(k) \ \cdots \ \mathbf{x}_P^T(k)]^T$. Notice that with this definition of H, the factorization (4.13) is no longer valid (an alternative definition that would keep (4.13) valid would be to use H' of dimension $m \times PN$).

We now collect M vector samples of the received signal during M symbol periods. Stacking these samples (in increasing order) in a polyphase $mMP \times 1$ vector, i.e., $X_M(k) = [\mathbf{x}^T(k) \;\; \mathbf{x}^T(k+1) \;\; \cdots \;\; \mathbf{x}^T(k+M-1)]^T$, we obtain the factorization

$$X_M(k) = \mathcal{H}S(k), \tag{4.20}$$

where $\mathcal{H}$ is the $mMP \times (N+M-1)$ matrix,

$$\mathcal{H} = \begin{bmatrix} \mathbf{0} & \boxed{H} & & \\ & \ddots & \ddots & \\ & & \boxed{H} & \\ & \boxed{H} & & \mathbf{0} \end{bmatrix} \tag{4.21}$$

and

$$S(k) = \begin{bmatrix} s(k+M-1) \\ \vdots \\ s(k-N+1) \end{bmatrix}. \tag{4.22}$$

Notice the block-Hankel structure of $\mathcal{H}$ (an equivalent formulation of (4.20) with a decreasing time index in X_M would result in a block-Toeplitz instead of a block-Hankel matrix—see [12, 20]).

If $\mathcal{H}$ is of full column rank, then

$$\text{Column span } (X) = \text{Column span } (\mathcal{H}), \tag{4.23}$$

and full column rank of $\mathcal{H}$ is guaranteed if $mMP \geq (N+M-1)$ and if the subchannel polynomials of H do not share a common root [12]. As will be seen later, the full column rank of $\mathcal{H}$ is an important property linked both to the identifiability and the equalizability of the channel.

Suppose we have M' polyphase vector samples of data and we wish to use these in blocks. We can then extend the data vector $X_M(k)$ to a block-Hankel matrix by left-shifting and stacking M' times:

$$\mathcal{X}_M = \begin{bmatrix} \mathbf{x}(k) & \mathbf{x}(k+1) & \cdots & \mathbf{x}(k+M'-M) \\ \mathbf{x}(k+1) & \mathbf{x}(k+2) & \cdots & \cdots \\ \cdots & \cdots & \cdots & \mathbf{x}(k+M'-2) \\ \mathbf{x}(k+M-1) & \cdots & \mathbf{x}(k+M'-2) & \mathbf{x}(k+M'-1) \end{bmatrix}, \tag{4.24}$$

which has size $mMP \times (M'-M+1)$. In terms of H and the transmitted symbol matrix, this augmented matrix can be expressed as

$$\mathcal{X}_M = \mathcal{H}\mathcal{S} = \tag{4.25}$$

$$\begin{bmatrix} 0 & \boxed{H} & & \\ & \ddots & \ddots & \\ & & \boxed{H} & \\ & & \boxed{H} & 0 \end{bmatrix} \begin{bmatrix} s(k+M-1) & \ddots & s(k+M'-2) & s(k+M'-1) \\ \ddots & \ddots & \ddots & s(k+M'-2) \\ s(k-N+2) & s(k-N+3) & \ddots & \ddots \\ s(k-N+1) & s(k-N+2) & \ddots & s(k+M'-M-N+1) \end{bmatrix},$$

where $\mathcal{H}$ is $mMP \times (N+M-1)$ and $\mathcal{S}$ is $(N+M-1) \times (M'-M+1)$. Equation (4.25) shows that the augmented data matrix admits a factorization into two matrices, a block-Hankel space-time channel matrix and a block-Toeplitz transmitted symbol matrix. This observation, too, is crucial to the blind identification of $\mathcal{H}$ from the observations $\mathcal{X}_M$.

In the MU case, we assume that multiple subscribers transmit their information signals towards the antenna array at the same base station. The MU-SIMO model is a straightforward extension of the SU-SIMO model. Assuming Q users, the symbol-rate sampled, received signal at the antenna array is the sum of the signals from Q subscribers, and using (4.19) we have

$$\mathbf{x}(k) = \sum_{q=1}^{Q} H_q \mathbf{s}_q(k). \tag{4.26}$$

A data model for the MU case will have Q channels corresponding to Q users, and we assume, for ease of exposition, that each user's channel impulse response spans N symbol periods. We interleave the sampled impulse responses of the Q users, sample by sample, taking the size of H to $mP \times QN$. Defining the Q-tuple symbol vector as $\mathbf{s}(k) = [s^{(1)}(k)s^{(2)}(k)\ldots s^{(Q)}(k)]^T$, where $s^{(i)}(k)$ denotes the kth symbol of ith user, we get the following signal model:

$$\mathcal{X}_M = \tag{4.27}$$

$$\begin{bmatrix} 0 & \boxed{H} & & \\ & \ddots & \ddots & \\ & & \boxed{H} & \\ & & \boxed{H} & 0 \end{bmatrix} \begin{bmatrix} \mathbf{s}(k+M-1) & \ddots & \mathbf{s}(k+M'-2) & \mathbf{s}(k+M'-1) \\ \ddots & \ddots & \ddots & \mathbf{s}(k+M'-2) \\ \mathbf{s}(k-N+2) & \mathbf{s}(k-N+3) & \ddots & \ddots \\ \mathbf{s}(k-N+1) & \mathbf{s}(k-N+2) & \ddots & \mathbf{s}(k+M'-M+N+1) \end{bmatrix},$$

so that $\mathcal{H}$ is $mMP \times Q(N+M-1)$, and $\mathcal{S}$ is $Q(N+M-1) \times (M'-M+1)$, and where the M shifts of H to the left are now each over Q positions. Again, as in the single-user case, the blind identification and equalization of the channel will be affected by the size and conditioning of $\mathcal{H}$.

4.2.2 Spatial and Temporal Signal Structure

Given the signal model at (4.25), an important question is whether the unknown channel $\mathcal{H}$ and data $\mathcal{S}$ can be determined from the observations $\mathcal{X}_M$. This question leads us to examine the underlying constraints on $\mathcal{H}$ and $\mathcal{S}$, which we call *structure*.

4.2.2.1 Spatial Structure

The spatial structure of H is apparent from (4.15). The vector $\mathbf{a}(\theta_l)$ lies on the *array manifold* $\mathcal{A}$, which is the set of array response vectors indexed by θ

$$\mathcal{A} = \{\mathbf{a}(\theta) \mid \theta \in \Theta\}, \tag{4.28}$$

where the set Θ is the set of all possible values of θ. Knowledge of $\mathcal{A}$ helps determine $\mathbf{a}(\theta_l)$. $\mathcal{A}$ includes the effect of array geometry, element patterns, interelement coupling, scattering from support structures, and objects near the base station. $\mathcal{A}$, when measured at the receiver baseband after digitization, includes the effects by cable and receiver gain/phase response, in-phase/quadrature (I-Q) imbalance, and analog-to-digital (A/D) converter errors. $\mathcal{A}$ is frequency-dependent and needs to be calibrated at multiple points within the operating band.

4.2.2.2 Temporal Structure

The temporal structure relates to the properties of the signal $u(t)$ and includes modulation format, pulse-shaping function, and symbol constellation. Some typical temporal structures are described below.

Constant Modulus (CM). In many wireless applications, the transmitted waveform has a constant envelope (e.g., in FM modulation). A typical example of a constant envelope waveform is the GMSK modulation used in the GSM cellular system, which has the following general form:

$$u(t) = e^{j(\omega t + \varphi(t))},$$

where $\varphi(t)$ is a Gaussian-filtered phase output of a minimum shift keyed (MSK) signal [23].

Finite Alphabet (FA). Another important temporal structure in mobile communication signals is the *finite alphabet*. This structure underlies all digitally modulated schemes. The modulated signal is a linear or nonlinear map of an underlying finite alphabet. For example, the IS-54 signal is a $\pi/4$-shifted DQPSK signal given by

$$u(t) = \sum_p A_p g(t - pT) + j \sum_p B_p g(t - pT), \tag{4.29}$$

where

$$A_p = \cos(\varphi_p), \quad B_p = \sin(\varphi_p), \quad \varphi_p = \varphi_{p-1} + \Delta\varphi_p,$$

$g(\cdot)$ is the pulse shaping function (which is a square root raised cosine function in the case of IS-54), and $\Delta\varphi_p$ is chosen from a set of finite phase shifts $\left\{\frac{5\pi}{4}, \frac{3\pi}{4}, \frac{\pi}{4}, \frac{7\pi}{4}\right\}$ depending on the data $s(\cdot)$. This finite set of phase shifts represents the FA structure.

Distance from Gaussianity. The distribution of digitally modulated signals is not Gaussian,[2] and this property can be exploited to estimate the channel from higher-order statistical quantities such as cumulants. See, e.g., [7] and [16]. Clearly CM signals are non-Gaussian. These higher-order statistics (HOS) based methods are usually slower converging than those based on second-order statistics.

Cyclostationarity. As discussed in Chapter 3, recent theoretical results [5, 12, 22, 25] suggest that exploiting the *cyclostationary* characteristic of the communication signal can lead to algorithms requiring only second-order statistics to identify the channel H and therefore are a more attractive approach than HOS techniques.

It can be shown [2] that the continuous-time stochastic process $x(t)$ defined in (4.3) (assuming the fade amplitudes α_ℓ are constant) is cyclostationary. Moreover, the discrete sequence $\{x_i\}$ obtained by sampling $x(t)$ at the symbol rate $\frac{1}{T}$ is wide-sense stationary, whereas the sequence obtained by temporal oversampling (i.e., at a rate higher than $1/T$) or spatial oversampling (multiple antenna elements) is cyclostationary. The cyclostationary signal consists of a number of *phases* (polyphase components), each of which is stationary. A phase corresponds to a shift in the sampling point in temporal oversampling and different antenna element in spatial oversampling. The duality between temporal and spatial oversampling is illustrated in Figure 4.6.

The cyclostationary property of sampled communication signals carries important information about the channel phase, and this information can be exploited in several ways to identify the channel. The cyclostationarity property can also be interpreted as a *finite duration* property. Put simply, the oversampling increases the number of samples in the signal $\mathbf{x}(t)$ and phases in the channel H but does not change the value of the data for the duration of the symbol period. This oversampling is what allows $\mathcal{H}$ to become tall (more rows than columns) and full column rank. Also, the stationarity of the channel makes $\mathcal{H}$ Hankel (or rather,

[2]The distribution may, however, approach a Gaussian when constellation shaping is used for spectral efficiency [34].

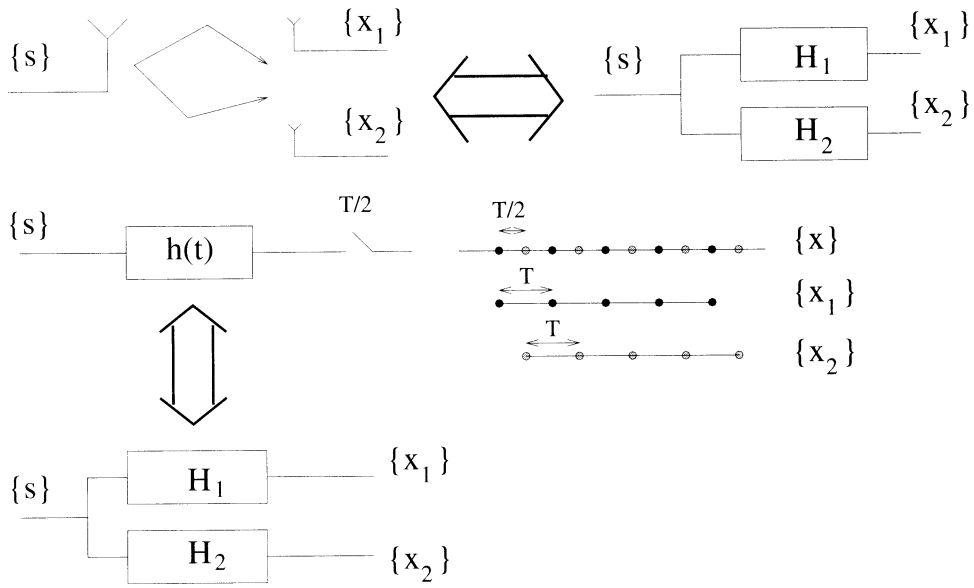

Figure 4.6 Antennas and/or oversampling result in polyphase SIMO channels.

block-Hankel). As indicated earlier, tallness and Hankel properties are key to the blind estimation of H.

The Temporal Manifold. Just as the array manifold captures spatial wavefront information, the *temporal manifold* captures the temporal pulse-shaping function information (see [32, 35]). We define the temporal manifold $\mathbf{k}(\tau)$ as the sampled response of a receiver to an incoming pulse with delay τ. The temporal manifold is a powerful structure for channel identification and tracking. Moreover, unlike the array manifold, it can be estimated with good accuracy since it depends only on our knowledge of the pulse-shaping function. Table 4.1 shows the duality between the array and the temporal manifold.

The different structures and properties inherent in the nature of the transmitted signals and the employed receivers in space-time processing are shown in Figure 4.7.

TABLE 4.1 The duality between the array and the time manifold

Manifold	Indexed by	Characterizes
Array	angle θ	antenna array response
Time	delay τ	transmitted pulse shape

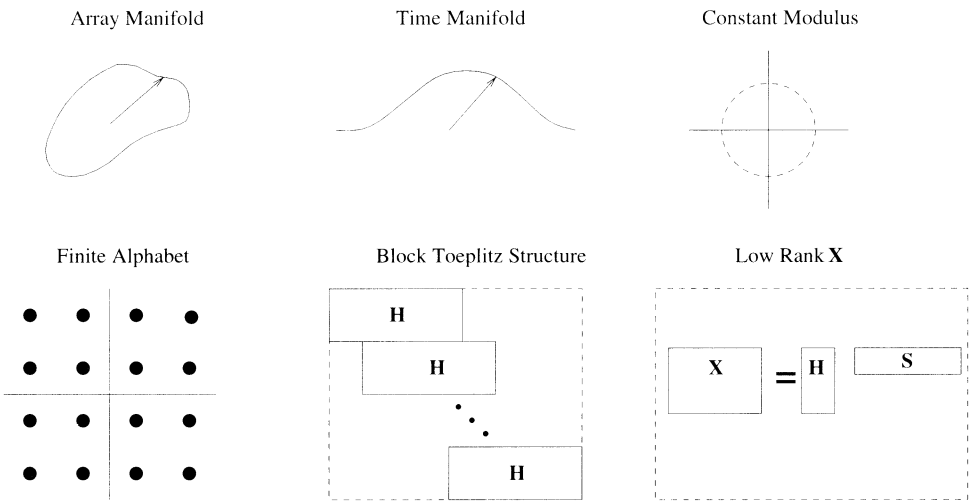

Figure 4.7 Space-time structures.

4.3 Channel Identification and Equalization

Given the model (4.25) or (4.27) and the received signal, the task of the receiver is to estimate the data S that were transmitted. This estimation is usually performed using one of two approaches. The first approach is to determine the channel H and then use a maximum-likelihood sequence estimator (MLSE) to find the data S. Another approach is to sidestep the channel estimation and invert or equalize the channel to reveal the data directly.

If we wish to equalize the channel, a key question is: What conditions on the channel make it invertible? On the other hand, if we wish to estimate the channel first, the corresponding question is under what conditions the received signal statistics alone can provide identification (this is called blind channel identification). Of course, the answers to these questions depend on the type of filters used for equalization and the type of signal statistics used for identification. We address these issues next, focusing on linear equalizers and blind identification based on second-order statistics (SOS).

4.3.1 Single-User Channels

We begin, in this section, with the equalization of single-user channels. The multi-user case is treated in the following section.

4.3.1.1 Conditions for Channel Equalization/Identification

We consider the problem of zero-forcing (ZF) equalization for an m-sensor receiver with a P-oversampled channel. Namely, we are interested in finding an equalizer of order M, $\mathbf{F}_M = [\mathbf{f}(0) \ \cdots \ \mathbf{f}(M-1)]^T$ (an $mMP \times 1$ vector), such that the following zero-forcing condition is satisfied for the equalizer output $y(k)$:

$$y(k) = \mathbf{F}_M^T X_M(k) \equiv s(k-\delta), \tag{4.30}$$

where $\delta \in [-M+1, N-1]$, which results according to (4.20) to

$$\mathbf{F}_M^T \mathcal{H} = [0 \cdots 0 \ \ 1 \ \ 0 \cdots 0], \tag{4.31}$$

where the position of the single non-zero element in the right-hand side of (4.31) depends of course on the choice of δ. To satisfy (4.31), the generalized Sylvester matrix $\mathcal{H}$ needs to be left-invertible, hence full column rank, which requires that it has at least as many rows as columns and that the different columns are linearly independent. This requirement results in the following two conditions:

(C1) $mMP \geq M + N - 1 \Rightarrow M \geq \underline{M} = \left\lceil \frac{N-1}{mP-1} \right\rceil$.

(C2) The polynomials $H_i(z)$, $i = 1, \ldots, mP-1$ corresponding to the different rows of H must have no common roots.

Therefore, zero-forcing equalization is indeed possible with a finite-length equalizer, provided that the received signal is oversampled (or received with multiple antennas) so as to satisfy (C1) and that the mP channel phases have no common zeros. Notice that this is still possible if only oversampling ($m = 1$, $P > 1$) or only antennas ($P = 1$, $m > 1$) are used. This fact was noticed by Slock in [20].[3]

The same conditions that hold for perfect noiseless ZF equalization turn out to be necessary and sufficient for the blind identification of a polyphase channel with the use of second-order-only (cyclostationary) statistics. The cyclostationarity of the sampled received signal is crucial in obtaining this result. The result was first obtained by Tong et al. in [25] and was stated as follows.

Theorem I. The channel transfer function $H(z)$ is uniquely determined (identified) by the cyclic spectrum of the oversampled channel output if and only if $H(z)$ does not have zeros uniformly spaced on a circle with separation of $2\pi/T$ radians.

In this theorem, $H(z) = \sum_{i=1}^{mP} z^{-i} H(z^{mP})$ represents the z-transform of the interleaved channel response. It is easy to show [28] that $H(z)$ has zeros equispaced on a circle if and only if the mP channel phase polynomials $H_i(z)$ have no common root (condition (C2) above).

[3]It turns out that similar conditions had appeared in a different context earlier (Massey and Sain [11]).

Hence, the common root condition is important for both the existence of finite-length linear equalizers and for SOS-based blind channel identification.

Whereas in theory it may be unlikely that all the subchannels share common roots, in practice they may have several roots that are very close to each other. This can make SOS-based methods ill conditioned. We show below that there exist some channel classes that will suffer from the common zeros problem and we present some approaches to overcome it.

4.3.1.2 Avoiding the Problem of Zeros in Common

According to Theorem I, SOS-based identifiability will fail when the phases of the different channels share common roots. Two questions are then of interest: how likely this is to happen and what can be done in practice to avoid it?

A partial answer to the first question was given in [28] and in [3]. In [28], it was observed that the following class of channels will always suffer from the zeros-in-common problem when oversampled in time:

- Class I: channels with delays that are all multiples of T

This case can be easily seen as follows. The impulse response of Class I channels will have the general form

$$h(t) = \sum_{l=0}^{L-1} \alpha_q g(t - lT); \tag{4.32}$$

hence, the ith phase $h_i(k) = h(t_0 + kT + (i-1)T/P$ will be given by

$$h_i(k) = \sum_{l=0}^{L-1} \alpha_q g_i(k - l), \tag{4.33}$$

where $g_i(k) = g(t_0 + kT + (i-1)/T)$. Taking the z- transform of (4.33) gives

$$H_i(z) = A(z)G_i(z), \tag{4.34}$$

where $A(z)$ is the z-transform of α_q. It is clear from (4.34) that the channel phases obtained from oversampling Class I channels have common zeros.

Some other channel classes that have the same identifiability problem when oversampled were reported in [3]. One of these classes is the following:

- Class II: band-limited channels with frequency nulls in $\left[-\frac{\pi(1-\beta)}{T}, \frac{\pi(1-\beta)}{T}\right]$, where β is the roll-off parameter

An example of such band-limited channels is shown in Figure 4.8.

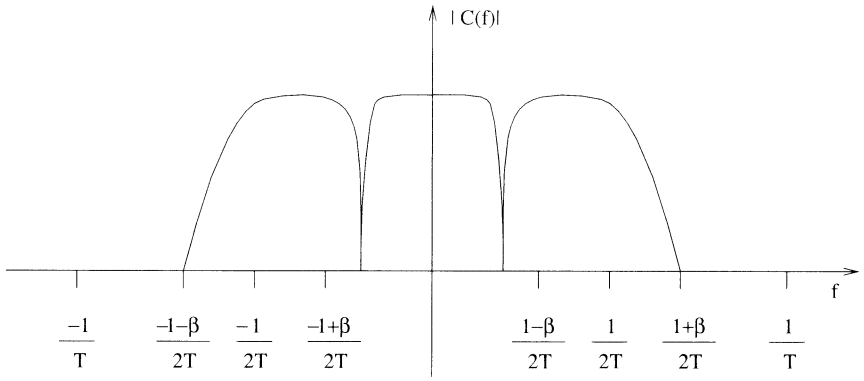

Figure 4.8 Typical example of a Class II band-limited channel.

The existence of the above channel classes suggests that the zeros-in-common identifiability problem is likely to arise in some practical cases. We now present some proposed approaches that avoid this problem.

Space-Time Oversampling. We consider first Class I channels. Instead of using time oversampling to obtain a polyphase channel (4.33), we could use space oversampling: the received signal is sampled at the symbol rate and received by an array of m sensors. Assuming a uniform linear array (ULA), the continuous-time impulse response corresponding to the ith sensor of the array would then be given by

$$\begin{aligned} h_i(t) &= \left(\sum_{l=0}^{L-1} \alpha_l e^{-j\frac{2\pi d}{\lambda}(i-1)\sin\theta_l} \delta(t - lT) \right) * g(t) \\ &= \left(\sum_{l=0}^{L-1} \alpha_l e^{-j\frac{2\pi d}{\lambda}(i-1)\sin\theta_l} g(t - lT) \right), \end{aligned} \tag{4.35}$$

where d is the interelement spacing, and λ is the wavelength of the carrier frequency. Defining the discrete impulse response of each antenna i as $h_i(k) = h_i(t)\big|_{t=t_0+kT}$ and the corresponding sampled pulse shaping function $g(k) = g(t)\big|_{t=t_0+kT}$, the z-transform of $h_i(k)$ is given by [18]

$$H_i(z) = \sum_{l=0}^{L-1} \gamma_{il} z^{-l} G(z), \tag{4.36}$$

where $\gamma_{il} = \alpha_l e^{-j\frac{2\pi d}{\lambda}(i-1)\sin\theta_l}$. According to (4.36), in the multiple sensors case, the common factor among the subchannels comes from the pulse shape (while in the oversampling case it comes from the multipath channel—cf. (4.34)). Now, if $g(t)$ is a Nyquist pulse (e.g., a pulse with raised cosine spectrum) and perfect synchronization has been achieved (t_0 is a multiple of T), then $G(z) = 1$. In this case, according to (4.36), the m subchannels will have no common roots as long as the arrival

angles of all the L multipaths are not the same or they do not correspond to array ambiguities. This reasoning establishes that for a Class I channel, the use of spatial instead of temporal oversampling helps avoid the identifiability problem. If synchronization is not perfect, then $G(z) \neq 1$; however, the identifiability problem can again be avoided if combined spatial and temporal oversampling is used [18].

We now consider the Class II channels, in which the identifiability problem comes from the fact that each frequency null in $[-\pi(1-\beta)/T, \pi(1-\beta)/T]$ gives rise, in the oversampled response, to a set of P roots that are located uniformly around the unit circle.

For example, we consider the class of multipath channels with two paths [3],

$$c(t) = \delta(t) + \delta\left(t - \frac{T}{(1-\eta)}\right), \eta > \beta, \tag{4.37}$$

which has a frequency null at $\omega = \frac{\pi(1-\eta)}{T}$ or $\omega = \frac{-\pi(1-\eta)}{T}$. We consider again the subchannels obtained from the m sensors of a uniform linear array. Following the steps similar to those used in arriving at (4.36), the ith antenna channel response is given in the z-domain by

$$H_i(z) = e^{-j\frac{2\pi d}{\lambda}(i-1)\sin\theta_0}(G(z) + \gamma_i G_\tau(z)), \tag{4.38}$$

where $g_\tau(k) = g(t-\tau)\,|_{t=t_0+kT}$. Observe that there is no common polynomial factor shared by the subchannels.[4] Thus, again, the use of an antenna array instead of oversampling can be used to allow the SOS identifiability of channels that would otherwise be unidentifiable.

Cyclostationarity Through Decision Feedback. A different approach to obtain cyclostationarity at the receiver without using temporal or spatial oversampling is the use of a decision-feedback equalizer (DFE) receiver. As we show below, after sufficient opening of the channel eye by the receiver, decision feedback can provide a polyphase signal that does not suffer from the zeros-in-common problem [14].

Consider the receiver shown in Figure 4.9, where symbol-rate sampling has been assumed:

When the switch is at position 2, the setup corresponds to a standard symbol-rate decision-feedback receiver. Assuming that the channel eye has been sufficiently opened (as is typically assumed in the analysis of DFEs), the following condition holds:

$$\hat{a}(k) = a(k-j), \tag{4.39}$$

where j is some inherent delay. In this case, the DFE receiver corresponds to the setup of Figure 4.9, where the switch is at position 1. One may now notice that the

[4]For $\tau = kT$, however, $G_\tau(z) = G(z)z^{-k}$, and it corresponds to a special case of the Class I channels.

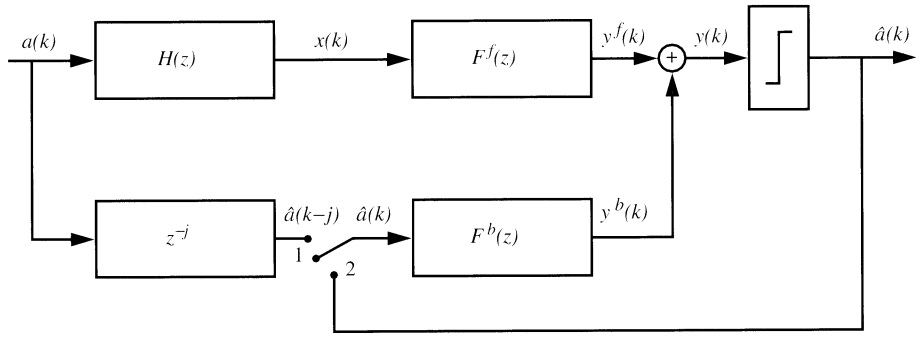

Figure 4.9 An equivalent DFE setup, assuming correct decisions.

vector input to the two filters $\tilde{\mathbf{x}}(k) = [x(k)\ \hat{a}(k)]^T$ can be seen as the output of the following single-input-two-output channel:

$$\begin{aligned} H_1(z) &= H(z) \\ H_2(z) &= z^{-j}. \end{aligned} \tag{4.40}$$

Therefore, the following theorem holds:

Theorem II. If (4.39) holds, the vector input $\tilde{\mathbf{x}}(k)$ to the feedforward and feedback filters is equal to the output of a single-input-two-output channel whose subchannels $H_1(z)$ and $H_2(z)$ have no common factor, except for a possible pure delay z^{-l}.

Based on the above theorem, the problem of zeros in common can be avoided with the use of decision feedback, provided that the channel eye has been sufficiently opened to provide correct decisions. A description of blind methods for DFE can be found in [14]. As compared to the above method of spatial oversampling, this approach requires less computational complexity since we need to compute only the values of a few coefficients in the feed-forward and feedback filters. On the other hand, the implementation of fully blind DFE techniques needs some care to guarantee cyclostationary structure (see [14]).

Transmission-Induced Cyclostationarity. An alternative approach to avoid the channel conditioning problem is to design communication signals that are cyclostationary prior to transmission. This cyclostationarity can either be artificially introduced by redundancy in transmission or arise naturally through the cyclostationary character of the transmitted signal. For example, in [27] it is shown that if one uses repetitive interleaving of a factor 2 at the transmitter, one obtains a SIMO channel model that does not suffer from identifiability problems. Of course, this is done at the cost of reduced bandwidth efficiency (if no extra bandwidth is used, this

approach will result in controlled ISI, whereas increasing the bandwidth will result in a repetition coding scheme). Similar results were presented in [1], where chip interleaving was used for the same reason prior to transmission in a CDMA system. The use of filter-bank-based precoding to induce cyclostationarity at the transmitter and avoid the zeros-in-common problem is also presented in [6]. Finally, in [8] it is shown that the SAT tone signal that is superimposed on the information bearing signal in the Advanced Mobile Phone Service (AMPS) analog cellular system used in North America also results in a cyclostationary transmitted signal.

4.3.2 Multiple-User Problem

Additional issues arise in multiuser problems, which we consider in the subsections that follow.

4.3.2.1 Joint ISI/CCI Cancellation

We consider again the general case of an m-antenna receiver with an oversampling factor of P. Assuming Q users, the ZF equalization condition is

$$\mathbf{F}_M^T X_M(k) = s^{(1)}(k - \delta), \tag{4.41}$$

where $\mathbf{F}_M^T$ and $X_M(k)$ are now $mMP \times 1$ and where we have assumed without loss of generality that we are interested in the recovery of the first user's signal (up to some delay). Using (4.27), this will give again

$$\mathbf{F}_M^T \mathcal{H} = [0 \ \cdots \ 0 \ 1 \ 0 \ \cdots \ 0] \qquad (1 \times Q(N + M - 1)). \tag{4.42}$$

Again, $\mathcal{H}$ needs to be left-invertible; hence, it is necessary that

$$M \geq \left\lceil \frac{Q(N-1)}{mP - Q} \right\rceil. \tag{4.43}$$

Again, (4.43) will not be sufficient to achieve perfect ISI/CCI cancellation unless the row polynomials of H are guaranteed to share no common roots [15, 21].

We may notice from (4.43) that even if pure temporal processing is used ($m = 1$), it is still theoretically possible to cancel perfectly both the channel ISI and CCI if oversampling is used ($P > 1$). However, in practice, this type of performance will be limited by the channel conditioning, as we discuss below.

4.3.2.2 Channel Condition and ISI/CCI Cancellation

The preceding ZF analysis for ISI and CCI canceling with linear filters did not address the important aspect of performance deterioration of the ZF equalizer in the presence of noise. It is well known that in the presence of noise, zero-forcing equalizers can cause severe noise amplification, especially when the channel has deep spectral notches. This picture also holds, broadly, for the oversampled case.

We now discuss how path parameters affect ZF equalizer performance in the ISI and CCI channel cases. Based on the previous discussion on ISI and CCI canceling, one might infer that the ISI and CCI cancellation appear to be much the same. A ZF equalizer cannot distinguish which interference it combats, and only the differences in the two channels distinguish them from each other.

However, there are some critical differences in the way the ISI and CCI channels are influenced by the channel parameters. For example, consider the case of L paths arriving at the antenna array with near equal delays ($\tau_1 \simeq \cdots \simeq \tau_L \simeq \tau$). If all paths come from the same user, this corresponds to a low delay spread case: the channel eye is open (assuming synchronization is achieved), and no equalization is needed.

On the other hand, if the paths correspond to different users, the different user channels are similar to each other, making ZF CCI cancellation very ill conditioned ($\mathcal{H}$ is near singular). This ill-conditioning causes severe noise amplification. It is clear from the above that in this case the ISI and CCI cancellation are affected by the path parameters in opposite ways!

Denoting by $\mathbf{F}$ the fractionally spaced ZF equalizer that completely nulls interference in the absence of noise and assuming the noise at the equalizer input to be white of variance σ_v^2, the noise variance at the equalizer output is given by

$$\sigma_o^2 = \sigma_v^2 ||\mathbf{F}||^2. \tag{4.44}$$

Hence, we can use the quantity $||\mathbf{F}||^2$ as a measure of noise amplification at the equalizer output.

To compare the performance between the ISI and the CCI case, we consider both an ISI and a CCI channel with two equipower signal paths with the interfering path arriving with a small delay equal to $\tau = T/20$. The received signal is of the form $x(t) = u(t) + u(t - T/20)$ in the ISI case and $x(t) = u_1(t) + u_2(t - T/20)$ in the CCI case. We have assumed linear modulation (see (4.2)) where $g(t)$ is a raised cosine pulse with roll-off parameter $\beta = 0.3$ (see [17]). The received signal is sampled with an offset of $\tau = T/20$ and oversampled by a factor of two. To evaluate the performance of zero-forcing equalization in this experiment, we have calculated for both cases the minimal-length zero-forcing equalizers that correspond to all possible cursor positions (δ in (4.30) or (4.41)).

In Figure 4.10, we have plotted the quantity $1/||\mathbf{F}||^2$ for each of the two cases (ISI and CCI). Notice from the figure both the effect on performance of the choice of δ and the dramatic noise amplification in the CCI case. As expected from the previous arguments, in the CCI case the two channels are very similar, leading to severe noise amplification, whereas in the ISI case the problem is well conditioned and good performance can be achieved.

We now consider a large delay-spread case: now the delay $\tau = 1.05T$ for both the ISI and the CCI channels. The performance in this case is shown in Figure 4.11.

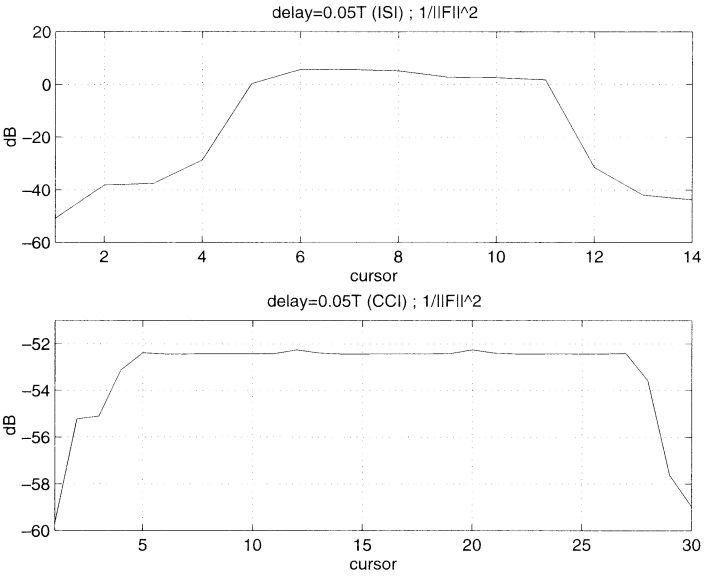

Figure 4.10 Performance comparison of ISI and CCI ZF equalizers (low delay spread).

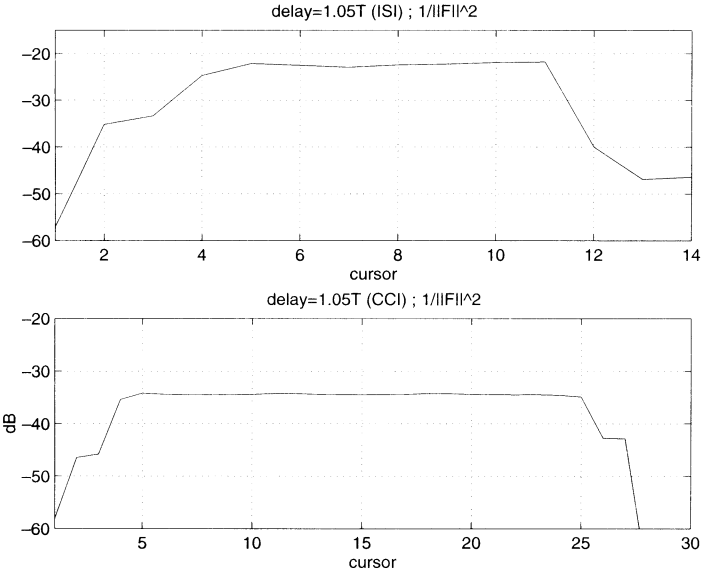

Figure 4.11 Performance comparison of ISI and CCI ZF equalizers (large delay spread).

Observe that whereas in the ISI case the performance is still superior, the gap between the two cases has reduced. Also, the performance of the ISI channel has considerably deteriorated. The first effect is due to the fact that now the two user channels in the CCI case are no longer similar; hence, the channel will be better conditioned. On the other hand, in the ISI case, the delay spread is now significant, leading to a performance reduction as compared to the earlier low delay spread.

These differences will vary depending on the channel and equalizer; e.g., if linear MMSE equalization is used instead of ZF equalization, the noise enhancement problem will be less pronounced. Also, if nonlinear equalization is used after the channels have been well identified, joint maximum-likelihood sequence detection will provide optimal performance irrespective of channel characteristics.

4.4 Blind Techniques

To this point, we have studied channel identifiability, equalizability, and the ISI/CCI cancellation problem. However, we have not yet addressed the important question of *how* signal recovery can be achieved. In the following discussion, we present two approaches for blind signal recovery from the channel output data in the multiple-user channel case. The single-user problem can be seen as a special case of this problem and will not be addressed in this chapter.

As derived in Section 4.2, if the channel is FIR, then the oversampled output signal can be written as

$$\mathcal{X} = \mathcal{H}\mathcal{S}.$$

The objective is to blindly identify $\mathcal{S}$.

A number of properties of the signal can be used, as was listed in Section 4.2. In particular, in this section we use the following properties.

1. The *fixed symbol rate* of the signals (equivalent to the finite duration property mentioned in Section 4.2.2.2), which allows one to obtain independent linear combinations of the same symbols by using oversampling and/or multiple antennas (assuming linear modulation). This property gives rise to the Toeplitz structure of $\mathcal{S}$ and is due to the (assumed) *time invariant* nature of the channel.
2. The *constant modulus* (CM) of the signals or their *finite alphabet* (FA).

We begin with the presentation of a block technique that makes use of the finite duration and FA properties. Then, we present a recursive technique that relies on the CM property.

4.4.1 Block Methods

The method presented below consists of two steps. The first step is a straightforward extension from scalars to vectors of the blind single-user equalization algorithm proposed by Moulines et al. in [12] and by Slock in [20] and discussed in Chapter 3. At this point, the ISI caused by the channel is removed and the input signals are synchronized. However, the symbol sequences can be determined only up to a fixed linear combination of them. This problem can then be treated with the methods proposed in [10, 30, 31].

4.4.1.1 Linear Data Model

To describe the FIR-MIMO (multiple-input multiple-output) scenario, consider the linear data model as detailed in Section 4.2, which we repeat here for convenience. Assuming m antennas, P times oversampling, and an equalizer length of M symbols, the MP-dimensional complex-valued data vectors $\mathbf{x}_k$ received at the antenna array during M' symbol periods are collected in the $MmP \times (M' - M + 1)$ block-Hankel matrix

$$\mathcal{X}_M = \begin{bmatrix} \mathbf{x}_0 & \mathbf{x}_1 & \cdots & \mathbf{x}_{M'-M} \\ \mathbf{x}_1 & \mathbf{x}_2 & \cdots & \cdots \\ \cdots & \cdots & \cdots & \mathbf{x}_{M'-2} \\ \mathbf{x}_{M-1} & \cdots & \mathbf{x}_{M'-2} & \mathbf{x}_{M'-1} \end{bmatrix} \tag{4.45}$$

(see (4.24)). Let N_j be the channel length of the qth user. With Q users and a maximum channel length of $N = \max_q N_q$ symbols per channel, $\mathcal{X}$ has a factorization (Section 4.2)

$$\mathcal{X}_M = \mathcal{H}\mathcal{S} = \begin{bmatrix} 0 & H & & \\ & \ddots & \ddots & \\ & & \ddots & H \\ H & & & 0 \end{bmatrix} \begin{bmatrix} \mathbf{s}_{M-1} & & \mathbf{s}_{M'-2} & \mathbf{s}_{M'-1} \\ \ddots & \ddots & \ddots & \mathbf{s}_{M'-2} \\ \mathbf{s}_{-N+2} & \mathbf{s}_{-N+3} & \ddots & \ddots \\ \mathbf{s}_{-N+1} & \mathbf{s}_{-N+2} & \ddots & \mathbf{s}_{M'-M-N+1} \end{bmatrix}$$

where we recall that $\mathcal{H}$ is an $MmP \times Q(N + M - 1)$ block-Hankel matrix, and $\mathcal{S}$ is a $Q(N + M - 1) \times (M' - M + 1)$ block-Toeplitz, finite alphabet matrix. The block H contains the impulse response of the channel, convolved with the modulating pulse shape function; $\mathbf{s}_k$ is a $Q \times 1$ vector containing the symbols transmitted by the Q users in the kth interval. For digital sources, the entries of $\mathbf{s}_k$ belong to a specific alphabet Ω, such as $\Omega = \{\pm 1\}$ for BPSK signals.

If MmP is large enough and $\mathcal{H}$ has full column rank, then $\mathcal{X}$ is rank-deficient and is expected to have rank

$$Q_{\mathcal{X}} = Q(N + M - 1). \tag{4.46}$$

Our goal is to factor $\mathcal{X}_M$ into $\mathcal{H}$ and $\mathcal{S}$ with the indicated structures as above. The *necessary* conditions for $\mathcal{X}_M$ to have a unique factorization $\mathcal{X}_M = \mathcal{H}\mathcal{S}$ are that $\mathcal{H}$ is a "tall" matrix and $\mathcal{S}$ is a "wide" matrix, which for $N > 1$ leads to

$$\begin{aligned} mP &> Q \\ M &\geq \frac{QN - Q}{mP - Q} \\ M' &> QN + (Q+1)(M-1). \end{aligned} \tag{4.47}$$

The common root condition mentioned in the single-user case now extends to the condition that H is "irreducible and column reduced." (See also (4.43).) Given sufficient data, only $mP > Q$ poses a fundamental identification restriction since M and M' are usually large enough.

Note that these conditions are *not sufficient* for $\mathcal{H}$ and $\mathcal{S}$ to have full rank. One case where $\mathcal{H}$ does not have full rank is when the channels do not have equal lengths, in which case the rank of $\mathcal{X}$ is at most $\sum N_q + Q(M-1)$.

4.4.1.2 Blind Multiuser Identification

The blind FIR-MIMO identification problem may be stated as a matrix factorization problem: given $\mathcal{X}$, find factors $\mathcal{H}$ and $\mathcal{S}$ with the indicated structure.

Suppose that the conditions (4.47) are satisfied and that $\mathcal{H}$ has full column rank $Q(N+M-1)$. Then, $\text{row}(\mathcal{X}) = \text{row}(\mathcal{S})$, so that we can determine the row span of $\mathcal{S}$ from that of $\mathcal{X}$. The first step of the algorithm is to compute an orthonormal basis $\hat{V}$ of $\text{row}(\mathcal{X})$. The next step is to find linear combinations of the rows of $\hat{V}$ such that the result both belongs to the finite alphabet (FA) and has a Toeplitz structure.

Forcing the Toeplitz Property: Subspace Intersections. A standard procedure to find $\mathcal{S}$ as a block-Toeplitz matrix with $\text{row}(\mathcal{S}) = \text{row}(\mathcal{X})$ (but not forcing the FA property) is to rewrite this as

$$\begin{array}{llllll} [\mathbf{s}_{M-1} & \mathbf{s}_M & \cdots & \mathbf{s}_{M'-1}] & \in & \text{row}(\mathcal{X}) \\ [\mathbf{s}_{M-2} & \mathbf{s}_{M-1} & \cdots & \mathbf{s}_{M'-2}] & \in & \text{row}(\mathcal{X}) \\ & & & & \vdots & \\ [\mathbf{s}_{-N+1} & \mathbf{s}_{-N+2} & \cdots & \mathbf{s}_{M'-N-M+1}] & \in & \text{row}(\mathcal{X}). \end{array} \tag{4.48}$$

These conditions can be aligned to apply to the same block-vector in several ways. We choose to work with

$$S := [\mathbf{s}_{-N+1} \;\; \mathbf{s}_{-N+2} \;\; \cdots \;\; \mathbf{s}_{M'-1}].$$

Let $\hat{V}$ be a basis for $\text{row}(\mathcal{X})$.

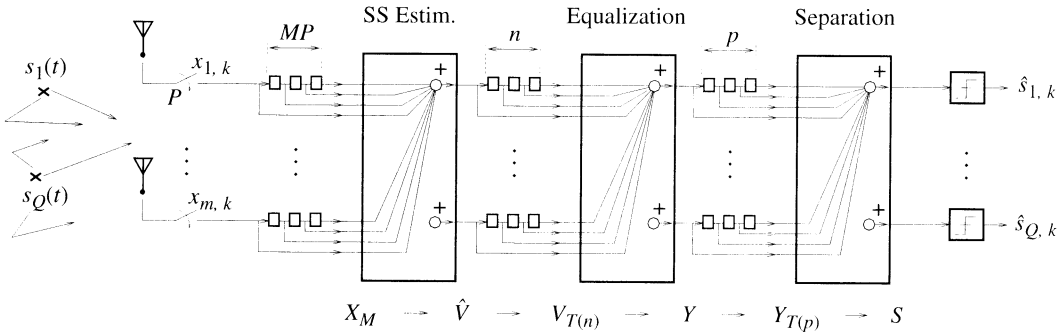

Figure 4.12 Multistage equalization/separation filter.

The conditions (4.48) can be transformed into

$$\begin{aligned} S &\in \operatorname{row} \hat{V}^{(1)}, & \hat{V}^{(1)} &:= \begin{bmatrix} \hat{V} & \mathbf{0} \\ \mathbf{0} & I_{N+M-2} \end{bmatrix}, \\ S &\in \operatorname{row} \hat{V}^{(2)}, & \hat{V}^{(2)} &:= \begin{bmatrix} \mathbf{0} & \hat{V} & \mathbf{0} \\ 1 & \mathbf{0} & \mathbf{0} \\ \mathbf{0} & \mathbf{0} & I_{N+M-3} \end{bmatrix}, \\ &\vdots \\ S &\in \operatorname{row} \hat{V}^{(N+M-1)}, & \hat{V}^{(N+M-1)} &:= \begin{bmatrix} \mathbf{0} & \hat{V} \\ I_{N+M-2} & \mathbf{0} \end{bmatrix}. \end{aligned} \tag{4.49}$$

Indeed, the identity matrices in each $\hat{V}^{(k)}$ reflect the fact that, at that point, there are no range conditions on the corresponding entries of $\mathbf{s}$. Thus, S is in the intersection of the row spans of $\hat{V}^{(1)}$ until $\hat{V}^{(N+M-1)}$, and we have to determine a basis for the intersection of a set of given subspaces. If all channel lengths are equal, then we expect to have Q signal sequences in the intersection.

To compute the intersection, we can use the fact that, for *orthonormal* bases $\hat{V}^{(k)}$ as we have in (4.49), the subspace intersection is obtained by computing the singular-value decomposition (SVD) of a stacking of all the basis vectors or, more conveniently, (for n intersections, $n = N + M - 1$) by an SVD of

$$V_{T(n)} := \begin{bmatrix} \hat{V} & & \mathbf{0} \\ & \hat{V} & \\ & \ddots \quad \ddots & \\ \mathbf{0} & \hat{V} & \\ J_1 & \mathbf{0} & \\ \mathbf{0} & & J_2 \end{bmatrix} \begin{matrix} \\ \\ \\ \\ \\ \\ \end{matrix} n, \tag{4.50}$$

where the n copies of $\hat{V}$ are each shifted over one entry, and

$$J_1 = \begin{bmatrix} \sqrt{n-1} & & 0 \\ & \ddots & \\ & & \sqrt{2} \\ 0 & & 1 \end{bmatrix}, \quad J_2 = \begin{bmatrix} 1 & & 0 \\ & \sqrt{2} & \\ & & \ddots \\ 0 & & \sqrt{n-1} \end{bmatrix}.$$

The matrices J_1, J_2 summarize the identity matrices present in (4.49), which is possible because we are interested only in row spans.

The estimated basis for the intersection (hence, for S) is given by the right singular vectors of $V_{T(n)}$ that correspond to the *large* singular values of $V_{T(n)}$: those that are close to $\sqrt{n}$. This subspace intersection algorithm has complexity $\mathcal{O}(Q^2(N+M)^3M')$ and is linear in M'.

Let Y be a matrix containing the estimated basis for the row span intersection. For $n = N + M - 1$, this matrix ideally consists of Q row vectors. To find S itself (hence, $\mathcal{S}$ as well), we have to determine which linear combination of the basis vectors gives a finite alphabet structure. Effectively, the subspace intersections perform a blind equalization jointly on all signals, but their separation is done based on the FA property.

Forcing the FA Property. For a given matrix Y, the iterated least-squares algorithms ILSP/E/F [24], and the constant modulus algorithm RACMA [29] (for BPSK or QPSK) solve the factorization

$$(Y = AS\text{: } A, S \text{ full rank}, [S]_{ij} \in \Omega), \tag{4.51}$$

where Ω is a prespecified finite alphabet, and A is any resulting nonsingular matrix.

Since the factorization $\mathcal{X} = \mathcal{H}\mathcal{S}$ is of the form (4.51), we could, in principle, use the ILSP or RACMA algorithm directly on $\mathcal{X}$. However, $\mathcal{X}$ is generally a large matrix with many rows, limiting the performance of ILSP (mainly in the context of finding *all* independent signals) and giving an unacceptably large computational complexity in RACMA. A second problem is that the algorithm does not force the Toeplitz structure of $\mathcal{S}$. After finding a candidate $\mathcal{S}$, we must compare the rows and detect which rows are shifted copies (echos) of other rows.

Detection of Q and L. If $\mathcal{H}$ and $\mathcal{S}$ have full column rank and row rank, respectively, then the rank of $\mathcal{X} = \mathcal{X}_M$ is $Q_{\mathcal{X}} := Q(N + M - 1)$. (See (4.46).) In principle, the number of signals Q can be estimated by increasing the blocking factor M of $\mathcal{X}_M$ by one and looking at the increase in rank of $\mathcal{X}_M$. This property provides a useful detection mechanism even if the noise level is quite high since it is independent of the actual (observable) channel length $\hat{N}$. Furthermore, the property still

holds if all channels do not have equal lengths. If they do, then N can be estimated from the estimated rank of $\mathcal{X}_M$, $\hat{Q}_{\mathcal{X}}$, and the estimated number of signals, $\hat{Q}$, by $\hat{N} = \hat{Q}_{\mathcal{X}}/\hat{Q} - M + 1$.

If the channels do not have equal length, but, say, lengths N_{ql}, then $\mathcal{H}$ is not full rank and a modification of the algorithm for estimating $\mathcal{S}$ is necessary. The approach in this case is to base the number of intersections on the *shortest* channel length among all sources. Doing so will equalize the corresponding channel and partially equalize the others. The remaining equalization is best carried out by means of the finite alphabet property. The details of this scheme are in [24]. Blind equalization is notoriously hard when channels have ill-conditioned and differing lengths.

4.4.2 Recursive Methods

We now summarize a recursive approach based on the CM property of the transmitted signals. Assuming Q users, we consider a linear $mM \times Q$ spatio-temporal equalization structure

$$\mathbf{F} = [F_1 \cdots F_Q],$$

where F_q, $q = 1,\ldots, Q$, denotes the filter corresponding to the qth signal. Then, the $Q \times 1$ equalizer output at time instant k can be written as

$$\mathbf{y}(k) = \mathbf{F}^T(k)X(k), \tag{4.52}$$

where $X(k) = [\mathbf{x}^T(k) \ \cdots \ \mathbf{x}^T(k + M - 1)]^T$, with $\mathbf{x}(k) = [x_1(k) \ \cdots \ x_m(k)]^T$. The MU-CM algorithm [15] is a simple blind technique to determine the coefficients of the spatio-temporal equalizer $\mathbf{W}$. We can set up a standard CM cost function and derive a set of coupled CM recursions that converge to the desired S-T equalizers. Global convergence to optimal settings can be guaranteed under most conditions.

The algorithm minimizes the following criterion:

$$\min_{\mathbf{F}} J(\mathbf{F}) = E\sum_{j=1}^{Q}\left(|y_j|^2 - 1\right)^2 + 2\sum_{l,n=1;\, l\neq n}^{Q}\ \sum_{\delta=\delta_1}^{\delta_2} |r_{ln}(\delta)|^2, \tag{4.53}$$

where $r_{ln}(\delta)$ is the cross-correlation function between users l and n defined as

$$r_{ln}(\delta) = E\left(y_l(k)y_n^*(k-\delta)\right), \tag{4.54}$$

and δ_1, δ_2 are integers that should be chosen in compliance with the channel delay spread in order to take into account all the achievable delays between different users. The cost function (4.53) is the sum of a CM term and a cross-correlation term:

the CM term penalizes the deviations of the equalized signals' magnitudes from a constant modulus, whereas the cross-correlation term penalizes the correlations between them. The corresponding stochastic-gradient algorithm has the form

$$\mathbf{F}(k+1) = \mathbf{F}(k) - \mu[\hat{\Delta}_1(k) \cdots \hat{\Delta}_Q(k)], \tag{4.55}$$

where

$$\Delta_j(k) = 4E\{(|y_j(k)|^2 - 1)y_j(k)\mathbf{X}^*(k)\} + 4 \sum_{l=1;\, l\neq j}^{Q} \sum_{\delta=\delta_1}^{\delta_2} r_{jl}(\delta) E\{y_l(k-\delta)\mathbf{X}^*(k)\}, \tag{4.56}$$

and $\hat{\Delta}_j$ is an estimate of Δ_j based on instantaneous values or sample averaging. Equation (4.55) describes a stochastic gradient algorithm derived from the MIMO "constant modulus" criterion (4.53) and is suitable for the spatio-temporal equalization of multiple user signals in the presence of both ISI and CCI. Simulations and analysis have shown its MMSE behavior at steady state, as well as its robustness to the power imbalance of different users.

The parameters employed are the equalizer length M, the number of users Q, and the step-size parameter μ. The number as well as the weight of the autocorrelation functions in the criterion (4.53) can be made variable. Equation (4.55) has a low computational complexity (depending on the number of terms present in the criterion as well as the length of the averaging window). Notice that (4.55) may reduce to the standard CMA 2-2 algorithm [26] in the case of one user ($Q = 1$).

4.5 Concluding Remarks

Space-time processing is a rapidly growing field that is still in its infancy. In this chapter, we have surveyed several aspects of this important research area that integrate and extend many of the concepts developed in earlier chapters. We hope that the results presented in the chapter will stimulate fresh research in this fascinating field.

References

[1] H. A. Cirpan and M. K. Tsatsanis. "Chip interleaving in direct sequence CDMA systems." *Proc. Int. Conf. Acoust., Speech, Signal Processing*, pages 3877–3880, Munich, Germany, April 1997.

[2] Z. Ding. "Blind channel identification and equalization using spectral correlation measurements, part I: frequency-domain analysis." In *Cyclostationarity in Communications and Signal Processing*, W. A. Gardner, ed., pages 417–436, New Jersey, USA, 1994.

[3] Z. Ding. "Characteristics of band-limited channels unidentifiable from second-order cyclostationary statistics." *IEEE Signal Processing Letters*, 3(5):150–152, May 1996.

[4] K. Feher. *Wireless Digital Communications*. Prentice Hall, Upper Saddle River, New Jersey, 1995.

[5] W. A. Gardner, editor. *Cyclostationarity in Communications and Signal Processing*. IEEE Press, New Jersey, USA, 1994.

[6] G. B. Giannakis. "Filter banks for blind channel identification and equalization ." *IEEE Signal Processing Letters*, 4(6):181–183, June 1997.

[7] G. B. Giannakis and J. M. Mendel. "Identification of nonminimum phase systems using higher order statistics." *IEEE Trans. Acoust., Speech, Signal Processing*, 37(3):360–377, March 1989.

[8] R. He and J. H. Reed. "Spectrum correlation characterization of AMPS signal with its application to interference rejection." *Proc. IEEE MILCOM*, October 1994.

[9] William C. Jakes, ed. *Microwave Mobile Communications*. John Wiley, New York, 1974.

[10] H. Liu and G. Xu. "Closed-form blind symbol estimation in digital communications." *IEEE Transactions on Signal Processing*, SP-43(11):2714–2723, November 1995.

[11] J. L. Massey and M. K. Sain. "Inverse of linear sequential circuits ." *IEEE Trans. Comput.*, pages 330–337, 1968.

[12] E. Moulines, P. Duhamel, J. F. Cardoso, and S. Mayrargue. "Subspace methods for the blind identification of multichannel FIR filters." *IEEE Trans. Signal Process.*, SP-43:516–525, 1995.

[13] Kaveh Pahlavan and Allen H. Levesque. *Wireless Information Networks*. John Wiley, New York, 1995.

[14] C. B. Papadias and A. Paulraj. "Decision-feedback equalization and identification of linear channels using blind algorithms of the Bussgang type." *Proc. Asilomar Conf. Signals, Systems, Computers*, Pacific Grove, California, October 1995, pages 335–340.

[15] C. B. Papadias and A. Paulraj. "A constant modulus algorithm for multi-user signal separation in presence of delay spread using antenna arrays." *IEEE Signal Processing Letters*, 4(6):178–181, June 1997.

[16] B. Porat and B. Friedlander. "Blind equalization of digital communication channels using higher order moments." *IEEE Trans. Acoust. Speech, Signal Processing*, SP-39(2):522–526, February 1991.

[17] J. G. Proakis. *Digital Communications*. McGraw-Hill, New York, 1983.

[18] V. U. Reddy, C. B. Papadias, and A. Paulraj. "Blind identifiability of certain classes of multipath channels from second-order statistics using antenna arrays." *IEEE Signal Processing Letters*, 4(5):138–141, May 1997.

[19] R. O. Schmidt. *A Signal Subspace Approach to Multiple Emitter Location and Spectral Estimation*. Ph.D. thesis, Stanford University, Stanford, California, 1981.

[20] D. T. M. Slock. "Blind fractionally-spaced equalization, perfect-reconstruction filter banks and multichannel linear prediction." *Proc. Int. Conf. Acoust., Speech, Signal Processing*, 4:585–588, Adelaide, Australia, April 1994.

[21] D. T. M. Slock. "Blind joint equalization of multiple synchronous mobile users using oversampling and/or multiple antennas." *Proc. Asilomar Conf. Signals, Systems, Computers*, Pacific Grove, California, October 1994.

[22] D. T. M. Slock and C. B. Papadias. "Further results on blind identification and equalization of multiple FIR channels." *Proc. Int. Conf. Acoust., Speech, Signal Processing*, 4:1964–1967, Detroit, Michigan, May 1995.

[23] R. Steele. *Mobile Radio Communications*. Pentech Press, 1992.

[24] S. Talwar, M. Viberg, and A. Paulraj. "Blind separation of synchronous co-channel digital signals using an antenna array. Part I. Algorithms." *IEEE Trans. Signal Process.*, 44(5):1184–1197, May 1996.

[25] L. Tong, G. Xu, and T. Kailath. "Blind identification and equalization of multipath channels: a time domain approach." *IEEE Trans. Inform. Theory*, 40(2):340–349, March 1994.

[26] J. R. Treichler and B. G. Agee. "A new approach to multipath correction of constant modulus signals." *IEEE Trans. Acoust. Speech, Signal Processing*, ASSP-31(2):459–472, April 1983.

[27] M. K. Tsatsanis and G. B. Giannakis. "Cyclostationarity in partial response signaling: a novel framework for blind equalization." *Proc. Int. Conf. Acoust., Speech, Signal Processing*, pages 3597–3600, Munich, Germany, April 1997.

[28] J. K. Tugnait. "On blind identifiability of multipath channels using fractional sampling and second-order cyclostationary statistics." *IEEE Trans. Inform. Theory*, 41:308–311, Jan. 1995.

[29] A. J. van der Veen. "Analytical method for blind binary signal separation." *IEEE Trans. Signal Processing*, 45(4):1078–1082, April 1997.

[30] A. J. van der Veen, S. Talwar, and A. Paulraj. "Blind estimation of multiple digital signals transmitted over FIR channels." *IEEE Signal Process. Letters*, 2(5):99–102, May 1995.

[31] A. J. van der Veen, S. Talwar, and A. Paulraj. "Blind identification of FIR channels carrying multiple finite alphabet signals." *Proc. Int. Conf. Acoust., Speech, Signal Processing*, 2:1213–1216, Detroit, 1995.

[32] M. C. Vanderveen, C. Papadias, and A. Paulraj. "Joint angle and delay estimation (JADE) for multipath signals arriving at an antenna array." *IEEE Commun. Letters*, 1(1):12–14, January 1997.

[33] M. D. Yacoub. *Foundations of Mobile Radio Engineering*. CRC Press, Boca Raton, Florida, 1993.

[34] E. Zervas, J. Proakis, and V. Eyuboglu. "Effects of constellation shaping on blind equalization." *Proc. SPIE*, 1565:178–187, July 1991.

[35] A. J. Paulraj and C. B. Papadias. "Space-time processing for wireless communications." *IEEE Signal Processing Magazine*, 14(6):49–83, November 1997.

ACKNOWLEDGMENT

This research was supported in part by the Department of the Army, Army Research Office, under Grant No. DAAH04-95-1-0249. The views and conclusions expressed in this document are those of the authors and should not be interpreted as necessarily representing the official policies or endorsements, either expressed or implied, of the Army Research Office or the U.S. Government.